


Cancer Cell-Erythrocyte Hybrid Membrane Coated Gold Nanocages for Near Infrared Light-Activated Photothermal/Radio/Chemotherapy of Breast Cancer

This article was published in the following Dove Press journal:
International Journal of Nanomedicine

Mengqi Sun¹
Yuchen Duan²
Yumeng Ma³
Qingyuan Zhang ¹

¹Department of Medical Oncology, Harbin Medical University Cancer Hospital, Harbin, Heilongjiang, People's Republic of China; ²Department of Cardiology, The First Affiliated Hospital of Harbin Medical University, Harbin, Heilongjiang, People's Republic of China; ³Department of Ultrasound, The Second Affiliated Hospital of Harbin Medical University, Harbin, Heilongjiang, People's Republic of China

Background: The combination of radiotherapy (RT) and chemotherapy, as a standard treatment for breast cancer in the clinic, is unsatisfactory due to chemoradioresistance and severe side effects.

Methods and Results: To address these issues, a cancer cell-erythrocyte hybrid membrane-coated doxorubicin (DOX)-loaded gold nanocage (CM-EM-GNCs@DOX) was constructed for near-infrared light (NIR)-activated photothermal/radio/chemotherapy of breast cancer. CM-EM-GNCs@DOX inherited an excellent homologous target ability from the cancer cell membrane and an immune evasion capability from the erythrocyte membrane, together resulting in highly efficient accumulation in the tumor site with decreased clearance. Following the highly efficient uptake of CM-EM-GNCs@DOX in cancer cells, the RT efficacy was remarkably amplified due to the radiosensitization effect of CM-EM-GNCs@DOX, which reduced the needed radiotherapeutic dose. Importantly, with NIR irradiation, CM-EM-GNCs@DOX exerted a high photothermal effect, which not only ruptured CM-EM-GNCs@DOX to release DOX for precise and controllable chemotherapy, but also potentiated chemo/radiotherapy by photothermal therapy.

Conclusion: Therefore, a highly efficient and safe combined photothermal/radio/chemotherapy approach was achieved in vitro and in vivo by CM-EM-GNCs@DOX, which provided a promising strategy for treating breast cancer.

Keywords: gold nanocages, biomimetic, cancer cell-erythrocyte, radiation sensitization, combined therapies, breast cancer

Introduction

Breast cancer has emerged as one of the most common malignancies and seriously threatens the health of women worldwide.^{1,2} The combination of radiotherapy (RT) and chemotherapy is a standard treatment in the clinic because of their synergistic anticancer effects.^{3,4} Unfortunately, the combined therapies have been observed to display unsatisfactory therapeutic efficiency and severe side effects due to the chemoradioresistant microenvironment of tumor tissues as well as nonspecific injury from ionization radiation and chemotherapeutic drugs.⁵⁻⁸ Therefore, it is very important to develop novel strategies to improve chemo/radiotherapeutic outcomes and simultaneously reduce their adverse effects.

Correspondence: Qingyuan Zhang
Department of Medical Oncology,
Harbin Medical University Cancer
Hospital, Harbin, Heilongjiang, People's
Republic of China
Tel/Fax +86-0451-86298333
Email zhangqingyuan@hrbmu.edu.cn

Recently, various high-Z nanomaterials have been developed as radiosensitizers to increase the response of tumors to ionizing radiation.^{9–12} This radiosensitization strategy allows the use of low-dose radiation to achieve a higher therapeutic effect and a reduced burden of radiotherapy in the body. Additionally, photothermal therapy (PTT), which is based on photothermal agents to absorb near-infrared light and generate heat, has gained much research interest in cancer treatment because of its facile, controllable and noninvasive characteristics.^{13,14} More important, PTT has been considered an ideal adjuvant treatment to potentiate chemo/radiotherapies by improving blood perfusion in tumor tissues and changing the tumor-microenvironment.^{15–17} Therefore, this approach promises a highly efficient and safe effect in chemo/radiotherapy assisted by combining radiosensitization and photothermal therapy. However, there are still challenges to designing an elaborate system for simultaneously achieving tumor-targeted radiosensitization and tumor-specific chemotherapy as well as highly efficient PTT. The burgeoning advances of nanotechnology provide plausible strategies to address these issues. Gold nanocages (GNCs), as multifunctional nanoplatforms, are particularly emphasized in multimodal therapies for cancer. On the one hand, the tunable localized surface plasmon resonance (LSPR) properties of these materials enable them with great potential as photothermal therapeutic agents for the ablation of tumors with favorable photothermal effects.^{18,19} On the other hand, GNCs are promising radiosensitizers to improve the efficiency of radiation due to the enhanced absorption/emission of photoelectrons and Auger electrons.²⁰ Importantly, GNCs with hollow interiors and porous walls could be used to preload and deliver drugs into tumor tissues.^{21,22} Therefore, GNCs seem to be a promising nanoplatform for highly efficient and safe combined treatments of breast cancer. To date, the applications of GNCs on drug loading, radiosensitization and PTT have been revealed. However, their potential as triple agents for harnessing combined photothermal/chemo/radiotherapy has not yet reported. Moreover, the lack of tumor specificity, drug leakage and easy clearance by the immune system limit the clinical application of GNCs.

Currently, the use of cellular membranes for nanoparticle coating has emerged as an approach to endow nanoparticles with particular biointerfacing properties. For example, cancer cell membrane-camouflaged nanoparticles possess superb specificity to homologous cancer cells.²³ Erythrocytes cell membrane can increase the circulation

lifetime and improve the immune evading abilities of cloaked nanoparticles.²⁴ Stem cell-derived nanoparticles have good cancer targeting abilities.²⁵ Although promising, it is difficult to meet the increasingly complex tasks by using a single cell membrane coating approach. Hence, in this work, cancer cell membranes (CMs) and erythrocyte membranes (EMs) were fused to fabricate hybrid cell membranes (CM-EM). Then, CM-EM was coated onto doxorubicin (DOX)-loaded GNCs (GNCs@DOX) to form CM-EM coated GNCs@DOX (CM-EM-GNCs@DOX) for combined photothermal/chemoradiotherapy of breast cancer. The CM-EM-GNCs@DOX inherited a homologous targeting ability from the CMs and immune evasion capabilities from EMs, together leading to highly efficient accumulation in the tumor site. After cell membrane-mediated uptake, CM-EM-GNCs@DOX exhibited a remarkable radiosensitization effect on breast cancer. Furthermore, under NIR irradiation, CM-EM-GNCs@DOX exerted an excellent photothermal effect, which not only induced DOX release by disrupting the coated cell membranes, but also potentiated chemo/radiotherapy by PTT. Therefore, an outstanding antitumor effect and biosafety were achieved *in vitro* and *in vivo* (Scheme 1).

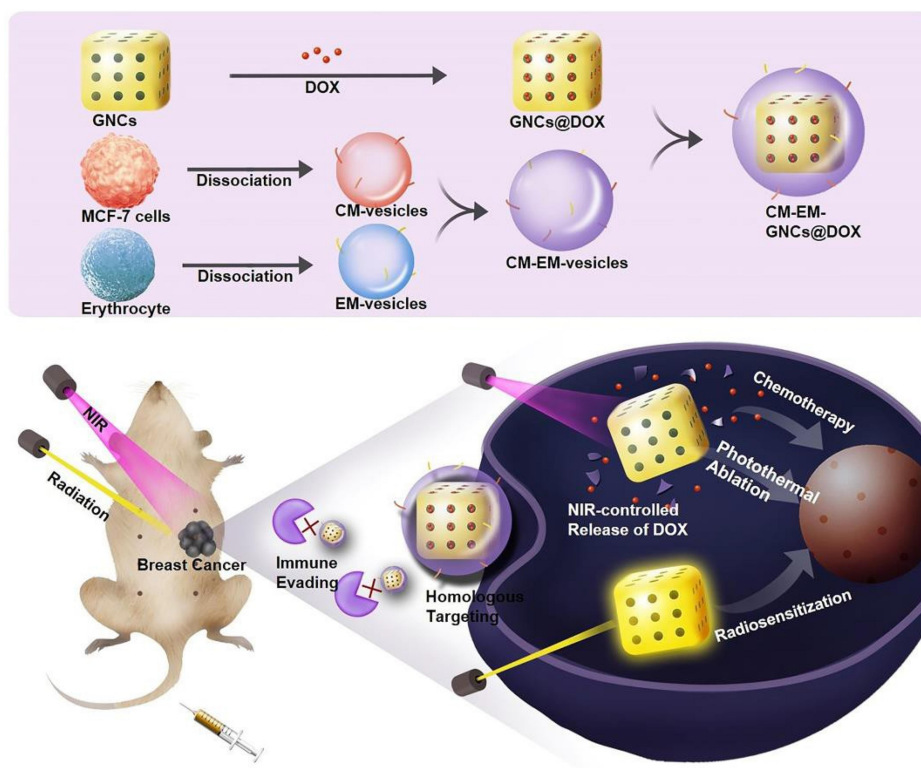
Methods

The Preparation of GNCs

GNCs were prepared via a replacement reaction between Ag nanocages and HAuCl₄ according to a previously reported method. Briefly, 1 mg of polyvinyl pyrrolidone (PVP) was dissolved in 5 mL of water. Then, 5 mg of Ag nanocages was mixed with the PVP solution. Next, the mixture was heated to 105 °C. After 20 min, 1 mM HAuCl₄ was dropwise injected into the mixture and refluxed for 20 min. Then, the mixture was naturally cooled down to room temperature. To obtain the GNCs, the solution was centrifuged at 10,000 r/min for 10 min and the products was washed repeatedly with ethyl alcohol and distilled water.

Preparation of CM-EM-Vesicles

Erythrocytes were trypsinized and centrifuged at 2000 r/min for 5 min. Then, an IKA T18 basic homogenizer was used to remove the nuclei of erythrocytes. Next, the enucleated erythrocytes were collected by differential centrifugation and suspended in 5 mL of deionized water. Subsequently, the collected products were sonicated for 15 min and extruded through 100 nm polycarbonate membranes by an Avanti Mini-Extruder (Avanti



Scheme 1 Cancer cell-erythrocytes hybrid membrane-coated gold nanocage with homologous targeting, immune evasion ability and NIR-triggered DOX release for combined photothermal/radio/chemotherapy of breast cancer.

Polar Lipids). Then, the obtained EM-vesicles were stored at 4 °C for further use. The CM-vesicles was extracted from MCF-7 cells and prepared using the same protocol. To prepare hybrid CM-EM-vesicles, the EM-vesicles were mixed with CM-vesicles under stirring for 10 min. Next, the mixture was sonicated and extruded through 100 nm polycarbonate membranes using an Avanti Mini-Extruder (Avanti Polar Lipids).

Preparation of CM-EM-GNCs

One milligram of GNCs was mixed with excess CM-EM-vesicles with sonication. Next, an Avanti Mini-Extruder (Avanti Polar Lipids) was used to extrude the mixture through 100 nm polycarbonate membranes. After processing with sonication for 10 min, CM-EM-GNCs were prepared. CM-GNCs and EM-GNCs were prepared using the same protocol.

The Loading and Release of DOX

Ten milligram of GNCs was mixed in 10 mL of a PBS solution of doxorubicin (DOX) with stirring overnight. Then, DOX-loaded GNCs (GNCs@DOX) were collected by centrifugation at 8000 r/min for 10 min. The

supernatant was collected to quantify the amounts of DOX by UV-vis spectroscopy. Then, the drug-loading content was calculated by the following equation: Drug-loading content = Mass of drug in NPs/Mass of drug. To investigate the DOX release behavior, 10 mg of GNCs@DOX was encapsulated in dialysis bags with a 5000 molecular weight cut-off and placed in 20 mL of PBS solution at 37 °C with shaking using a shaking table. At the designed time, the amount of released DOX was measured by UV-vis spectroscopy.

Cellular Uptake Assay

Human breast cancer cell line MCF-7 cells, human mammary epithelial cell line MCF10A cells and murine macrophage cell line RAW264.7 cells were cultured in RPMI1640 medium with 10% fetal bovine serum at 37 °C. No ethics committee permission was required for the use of MCF-7 cells, MCF 10A and RAW264.7 cells because these certificated cell lines were purchased from ATCC. MCF-7 cells, MCF 10A cells and RAW264.7 cells were seeded in 24-well plates at a density of 2×10^4 cells/well for 24 h. Then, the cells were coincubated with 20 µg/mL GNCs, CM-GNCs, EM-GNCs and CM-EM-GNCs for

6 h, respectively. Next, these cells were trypsinized and counted by a hemocytometer and dissociated in 100 μ L of formic acid (1 mol/L). Finally, the gold content in these cells was quantified by ICP-MS.

In vitro Cytotoxicity

MCF-7 cells were seeded in a 96-well plate at a density of 5×10^3 cells/well for 24 h. Then, various concentrations of CM-EM-GNCs@DOX (0, 2.5, 5, 10, 20 and 40 μ g/mL), GNCs, CM-EM-GNCs (equal to nanoparticle concentration in CM-EM-GNCs@DOX) and free DOX (equal to DOX concentration in CM-EM-GNCs@DOX) were coincubated with these MCF-7 cells for 24 h. Next, the cell viabilities were measured by a sulforhodamine B (SRB) assay. Briefly, trichloroacetic acid (20%, 100 mL) was added to the MCF-7 cells. After 3 h, the supernatant was removed. Then, 100 mL of SRB solution (0.4% w/v) was added. After 3 min, 200 mL of Tris-HCl was mixed with the solution to solubilize SRB. Last the optical density value of the solution was determined to measure the cell viabilities. To study the photothermal effect of these nanoparticles, an 808-nm laser at a power density of 50 mW/cm² was used to irradiate the abovementioned cells. Then, the cell viabilities were measured by the SRB assay. To study the radiosensitization effect of these nanoparticles and evaluate the combined therapeutic effect, a standard and flattening filter-free 6 MV X-ray (TrueBeam; Varian Medical System, Palo Alto, CA, USA) with a mean dose rate of 1 Gy/min was employed to perform radiotherapy. The MCF-cells were incubated with PBS and 20 μ g/mL CM-EM-GNCs @DOX as well as free DOX (equal to DOX concentration in CM-EM-GNCs@DOX), GNCs, CM-EM-GNCs (equal to nanoparticle concentration in CM-EM-GNCs@DOX) for 24 h and exposed with/without 808-nm laser (50 mW/cm²) and X-ray for 3 min. Then, the cell viabilities were measured by the SRB assay.

Intracellular Distribution of DOX

To evaluate the intracellular distribution of DOX, MCF-7 cells were coincubated with 10 μ g/mL CM-EM-GNCs @DOX and free DOX (equal to the amount of DOX loaded in CM-EM-GNCs@DOX) for 6 h. In the CM-EM-GNCs @DOX+NIR groups, an 808-nm laser was used to irradiate the MCF-7 cells at 1 h, 3 h and 5 h postadministration. Then, MCF-7 cells were stained with DAPI and observed using confocal microscopy. To quantify the cellular internalization of DOX, the MCF-7 cells were collected, and suspended in PBS. Then, the fluorescence intensity of DOX in each group was measured by a flow cytometry.

In vivo Therapeutic Effect

Twenty-gram female nude mice were bought from the Animal Experimental Center of Harbin Medical University and resided in a conventional animal housing facility. All the animal experimental protocols were approved by the Ethics Committee for the Use of Experimental Animals of Harbin Medical University. The experimental operation was carried out in agreement with the National Institute of Health Guide for the Care and Use of Laboratory Animals. These female nude mice were orthotopically injected with 5×10^6 MCF-7 cells into the mammary fat pads. When the tumors reached approximately 100 mm³, all the mice were randomized into the groups and intravenously injected with PBS, CM-EM-GNCs, free DOX, CM-EM-GNCs@DOX, CM-EM-GNCs @DOX plus NIR, RT, CM-EM-GNCs plus RT, and CM-EM-GNCs@DOX plus RT with NIR. The administration dosages of DOX, CM-EM-GNCs and CM-EM-GNCs @DOX were 0.5 mg/kg, 9.5 mg/kg and 10 mg/kg, respectively. In the RT groups, CM-EM-GNCs plus RT, and CM-EM-GNCs@DOX plus RT plus NIR, the mice were treated with 3 Gy of X-ray (1 Gy/min) by a 1.5 cm² radiation field after 24 h of intravenous administration. In the CM-EM-GNCs@DOX plus RT groups and the CM-EM-GNCs @DOX plus RT with NIR groups, an 808-nm laser (50 mW/cm²) was used to irradiate the tumor tissues for 3 min at 24 h and 48 h postinjection. All the tumors were measured by a digital caliper and the mice were weighed every 3 days. The tumor volume was calculated by the length \times width² \times 0.52. During the next 20 days, all the mice were sacrificed. These tumors was harvested and weighed, and serum was collected to measure the levels of alanine aminotransferase (ALT), aspartate aminotransferase (AST), phosphocreatine kinase (CK), creatinine (CRE) and blood urea nitrogen (BUN). The heart, liver, spleen, lung, and kidney were also harvested, fixed using 10% formalin, embedded in paraffin and stained with hematoxylin and eosin (HE).

Statistical Analysis

Student's *t*-test was used to analyze the differences between groups when comparing only two groups. $p < 0.05$ indicates a significant difference.

Results and Discussion

The gold nanocages (GNCs) were synthesized using a replacement reaction between silver nanocage and HAuCl₄ according to previous reports.²⁶ As shown in [Figure 1A](#) and [Figure S1](#), GNCs showed uniform

morphology and excellent monodispersity. The dynamic light scattering measurement in [Figure S2](#) revealed that their size distribution was approximately 50 nm. Then, doxorubicin (DOX) was encapsulated into the GNCs through electrostatic interactions, and the DOX loading content was 5.1%. To enhance the stability of GNCs with less DOX leak and improve their tumor targeting as well as immune evading abilities, hybrid cancer cell-erythrocyte membranes (CM-EM) was coated onto the surface of DOX-loaded GNCs (GNCs@DOX) by a top-down approach.²⁷ Briefly, cancer cell membranes (CMs) and erythrocyte membranes (EMs) were extracted from human breast cancer MCF-7 cells and human red blood cells, respectively. Then, the CMs and EMs were sonicated and extruded to yield vesicles. Finally, these vesicles were mixed and extruded with GNCs@DOX to form CM-EM-GNCs@DOX. The TEM image in [Figure 1B](#) presented a lipid bilayer shell with a thickness of approximately 5 nm on the surface of the GNCs. The DLS measurements also confirmed that the size of CM-EM-GNCs@DOX was larger than that of GNCs@DOX ([Figure 1C](#)). In addition,

the surface zeta potential of CM-EM-GNCs@DOX (-19.5 ± 0.7 mV) was similar to that of CM-EM-vesicles (-19.9 ± 0.4 mV) and lower than that of GNCs@DOX (-10.7 ± 0.8 mV) ([Figure 1C](#)), and the surface protein analysis of CM-EM-GNCs@DOX was consistent with the specific proteins of CMs and EMs identified by SDS-PAGE analysis ([Figure 1D](#)). These results indicated that CM-EM was successfully coated onto the GNCs@DOX.

We next investigated the localized surface plasmon resonance (LSPR) properties of CM-EM-GNCs in the absence of DOX by UV-vis spectrometry. As shown in [Figure 2A](#), similar LSPR properties were observed between GNCs and CM-EM-GNCs, indicating that the CM-EM coating did not obviously change the LSPR property of GNCs. Furthermore, CM-EM-GNCs exhibited a distinct characteristic absorption peak at a wavelength of 790 nm. The strong absorption of CM-EM-GNCs at the NIR region indicated their excellent photothermal effect. To evaluate the photothermal conversion effect of CM-EM-GNCs, an 808-nm laser at a power density of 50 mW/cm² was used to irradiate PBS solution of CM-EM-GNCs at various concentrations. As shown in [Figure 2C](#), the temperature of PBS without CM-EM-GNCs

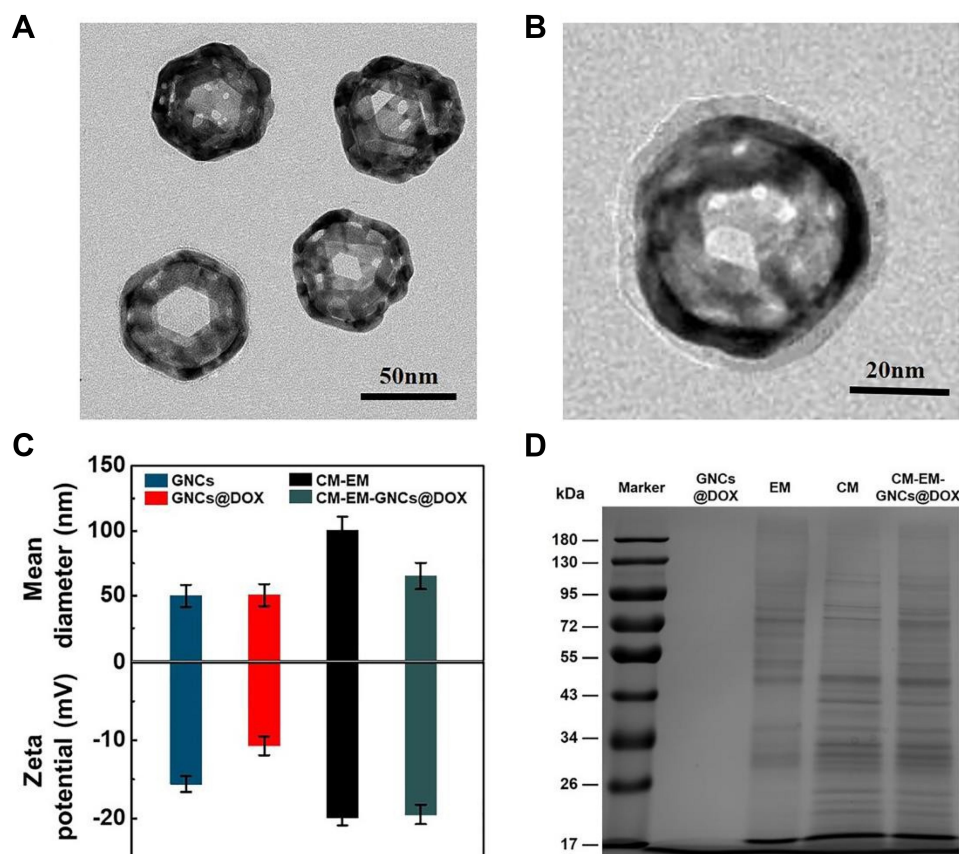


Figure 1 Characterization of CM-EM-GNCs. **(A)** TEM images of GNCs. **(B)** TEM images of CM-EM-GNCs. **(C)** Hydrodynamic size and zeta potential of GNCs, GNCs@DOX, CM-EM and CM-EM-GNCs@DOX. Mean \pm S. D.; (n = 3). **(D)** SDS-PAGE protein analysis of GNCs@DOX, EM, CM and CM-EM-GNCs@DOX.

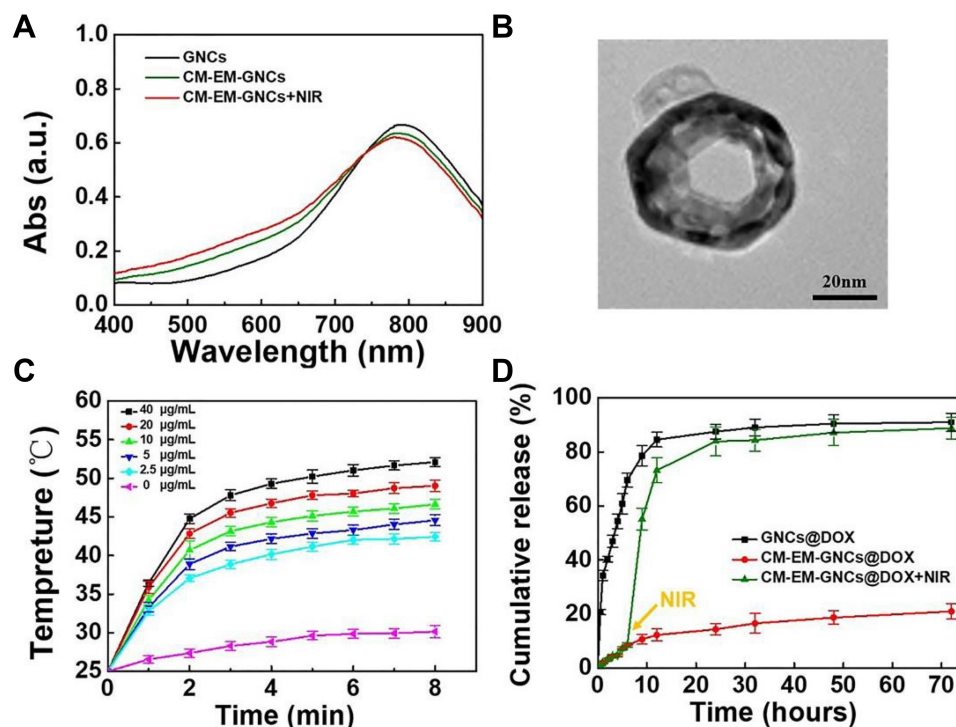


Figure 2 Photothermal properties and DOX release. (A) Vis-NIR spectra of GNCs, CM-EM-GNCs and CM-EM-GNCs after 3 min of irradiation by NIR. (B) TEM image of CM-EM-GNCs after 3 min of irradiation by NIR. (C) Temperature changes of different concentrations of CM-EM-GNC solution exposed to an 808-nm laser. (D) The DOX release behavior of GNCs@DOX and CM-EM-GNCs@DOX. The data are presented as the mean values \pm SD. (n=3).

only increased by 5 °C, whereas a concentration- and time-dependent increase was detected in CM-EM-GNCs solutions. At a concentration of 10 µg/mL with 3 min of NIR irradiation, the temperature reached 43.0 °C, which was critical for ablating cancer cells by thermal effects. In addition, CM-EM-GNCs showed a similar temperature increase with GNCs under NIR irradiation, indicating that the cell membrane coating did not lower the photothermal conversion ability of GNCs (Figure S3). Then, we investigated the photothermal stability of CM-EM-GNCs via UV-vis spectroscopy. As shown in Figure 2A, no observable LSPR shift of CM-EM-GNCs could be detected after exposure to NIR for 3 min, indicating the excellent photothermal stability of CM-EM-GNCs for repeated RTT treatments. Notably, the outside cellular membrane was disrupted by the photothermal effect, suggesting a controlled drug release ability of CM-EM-GNCs by NIR irradiation (Figure 2B). We next verified the DOX release behavior of CM-EM-GNCs@DOX under NIR irradiation. As shown in Figure 2D, without CM-EM coating, nearly 80% of DOX leaked from GNCs@DOX at the first 9 h. After coating with CM-EM, less than 20% of DOX was released within 24 h, indicating that the coating of cellular membranes could effectively improve the stability of the drug delivery system under the physiological conditions. Interestingly, when irradiated with NIR, CM-EM-GNCs@DOX exhibited a dramatically accelerated

DOX release from this point and over 80% DOX was ultimately released from CM-EM-GNCs@DOX. The NIR-induced DOX release behavior of CM-EM-GNCs@DOX would contribute to achieving precise chemotherapy at the desired time and location.

To investigate the effect of coated cell membranes on the cellular internalization behavior of these nanoparticles, we prepared single cell membrane-coated GNCs (CM-GNCs, EM-GNCs) as contrast and quantitatively determined the intracellular concentrations of nanoparticles after 6 h of cocultivation with human breast cancer MCF-7 cells, human mammary epithelial MCF 10A cells or RAW264.7 murine macrophages by ICP-MS. As shown in Figure 3, the gold signals in GNC-treated groups were slightly lower than those in the EM-GNC-treated groups and remarkably lower than those in the CM-GNC- and CM-EM-GNC- treated groups in the MCF-7 cells, whereas the uptake efficiency of CM-GNCs, EM-GNCs and CM-EM-GNCs was similar and slightly higher than that of GNCs in the MCF 10A cells. Notably, the gold signal in MCF-7 cells was 3.9-fold higher than that in MCF 10A cells in the CM-GNC-treated groups, while MCF-7 cells showed approximately 4.1-fold higher gold signal than MCF 10A cells after treatment with CM-EM-GNCs. These results indicated that CM-EM-GNCs possessed

better uptake efficiency in MCF-7 cells than in MCF 10A cells due to CM-mediated homogenous targeting. Although EM had a slightly increased effect on endocytosis with non-specificity in both MCF-7 cells and MCF 10A cells, it was found that EM coating could effectively decrease the phagocytosis of RAW264.7 cells. The excellent immune-escape abilities of CM-EM-GNCs would inhibit the clearance of macrophages and prolong the blood circulation time of these nanoparticles in the body.

To intuitively evaluate the chemotherapeutic effect of CM-EM-GNCs@DOX, we measured the cytotoxicity of free DOX, GNCs, CM-EM-GNCs and CM-EM-GNCs@DOX at different concentrations towards MCF-7 cells after 24 h incubation by SRB assay. As shown in Figure 4A, both GNCs and CM-EM-GNCs showed negligible cytotoxicity, indicating good biocompatibility of our prepared nanocarriers. Free DOX and CM-EM-GNCs@DOX displayed

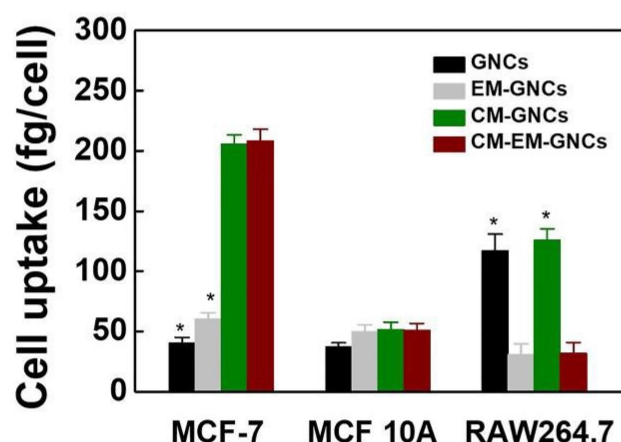


Figure 3 The cellular internalization of GNCs, EM-GNCs, CM-GNCs and CM-EM-GNCs in MCF-7 cells and MCF 10A cells as well as RAW264.7 cells. *P < 0.05 vs the CM-EM-GNC groups. The data are presented as the mean values \pm SD. (n = 3).

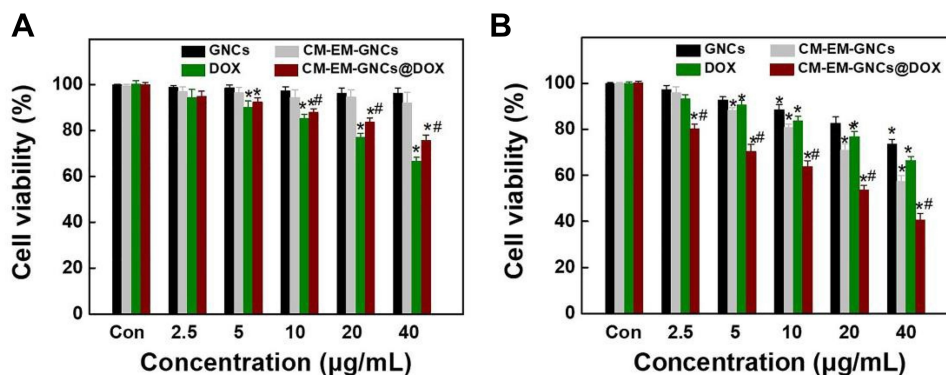


Figure 4 Cytotoxicity of CM-EM-GNCs@DOX under NIR irradiation. (A) Cell viabilities of MCF-7 cells after coincubation with various concentrations of GNCs, CM-EM-GNCs, GNCs@DOX and CM-EM-GNCs@DOX for 24 h. (B) Cytotoxicity of CM-EM-GNCs, GNCs@DOX and CM-EM-GNCs@DOX under NIR irradiation for 3 min. *P < 0.05 vs the Con groups; #P < 0.05 versus Dox groups. The data are presented as the mean values \pm SD. (n = 3).

concentration-dependent cytotoxicity towards MCF-7 cells. The cell death rate in the CM-EM-GNCs@DOX-treated groups was lower than that in the free DOX-treated groups, which might be due to the weak DOX release of CM-EM-GNCs@DOX. After irradiation with NIR, no obvious change was measured in the DOX-treated groups, whereas the killing effects of GNCs, CM-EM-GNCs and CM-EM-GNCs@DOX were remarkably improved (Figure 4B). The PTT efficiency of CM-EM-GNCs was superior to that of GNCs, which was due to the targeting effect of cellular membranes. We hypothesized that the excellent anticancer efficacy of CM-EM-GNCs@DOX originated not only from PTT effect, but also the accelerated release of DOX triggered by NIR. For verification, we detected the intracellular distribution of DOX after various treatments by confocal microscopy and flow cytometry. As shown in Figure 5A and B, without NIR irradiation, the fluorescence of DOX in CM-EM-GNCs@DOX-treated groups was weaker than that in free DOX-treated groups. When irradiated by NIR, CM-EM-GNCs@DOX showed enhanced intracellular DOX fluorescent signals, which was even higher than that with free DOX due to high efficiency of DOX delivery assisted by CM-EM-GNCs@DOX. These results confirmed that our CM-EM-GNCs@DOX possessed an excellent PTT effect and NIR-induced chemotherapy.

We next explored the radiosensitization effect of our nanoplatform and evaluated the anticancer effect of combined photothermal/radio/chemotherapy in vitro. As shown in Figure 6A, X-ray alone without any nanoparticles could only induce 37.2% death of MCF cells. After treatment with CM-EM-GNCs and GNCs, the radiotherapeutic efficiency was obviously improved. CM-EM-GNCs combined with RT displayed stronger therapeutic efficacy than GNCs combined with RT due to cell membrane-mediated targeting.

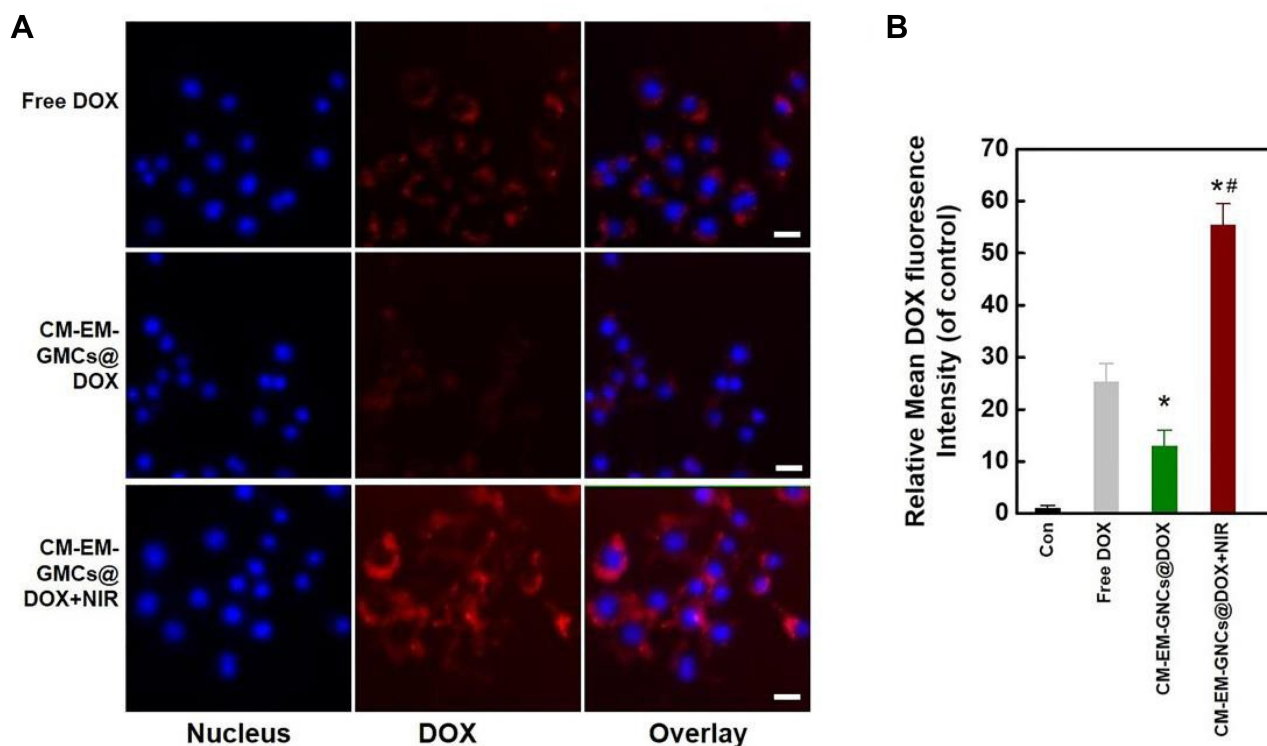


Figure 5 DOX release behavior of CM-EM-GNCs@DOX. **(A)** Confocal microscopy images of MCF-7 cells after incubation with free DOX or CM-EM-GNCs@DOX for 6 h with or without 3 min of NIR irradiation. **(B)** Quantitative analysis of the cellular internalization of DOX by flow cytometry. * $P < 0.05$ vs the DOX groups; # $p < 0.05$ versus CM-EM-GNCs@DOX groups. The data are presented as the mean values \pm SD; (n = 3).

These results indicated the superb radiation enhancement of our CM-EM-GNCs. Notably, CM-EM-GNCs@DOX plus NIR with RT showed a higher anticancer effect than CM-EM-GNCs@DOX plus NIR and CM-EM-GNCs@DOX plus RT, indicating an excellent combined photothermal/radio/chemotherapy by CM-EM-GNCs@DOX. To further investigate the long-term therapeutic effects of our CM-EM

-GNCs@DOX, clonal ability of MCF cells after various treatments was measured. Consistent colony formation inhibition with the SRB assay was observed (Figure 6B). These results indicated that CM-EM-GNCs@DOX could integrate photothermal/chemo/photothermal therapy with controllability and high efficiency for the treatment of breast cancer.

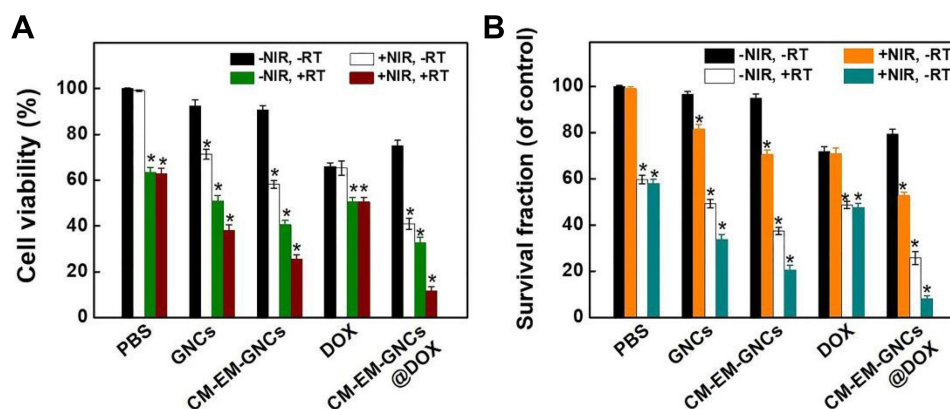


Figure 6 Combined photothermal/radio/chemotherapy of CM-EM-GNCs@DOX in vitro. **(A)** Cell viability of MCF-7 cells after treatment with PBS, GNCs, CM-EM-GNCs, free DOX and CM-EM-GNCs@DOX with (+) or without (-) X-ray or NIR irradiation. **(B)** Colony formation assay of MCF-7 cells after treated with PBS, GNCs, CM-EM-GNCs, free DOX and CM-EM-GNCs@DOX with (+) or without (-) X-ray or NIR irradiation. * $P < 0.05$ vs -NIR, -RT groups; The data are presented as the mean values \pm SD; (n = 3).

Encouraged by these findings, we further explored the potential of CM-EM-GNCs@DOX combined with NIR and RT to inhibit tumor growth in vivo. The biodistribution of these nanoparticles in tumor tissues and major organs was

investigated after 24 h intravenous administration by ICP-MS. As shown in Figure 7A, these nanoparticles predominantly accumulate in the tumor tissues and the reticuloendothelial system including the liver, spleen, and kidneys.

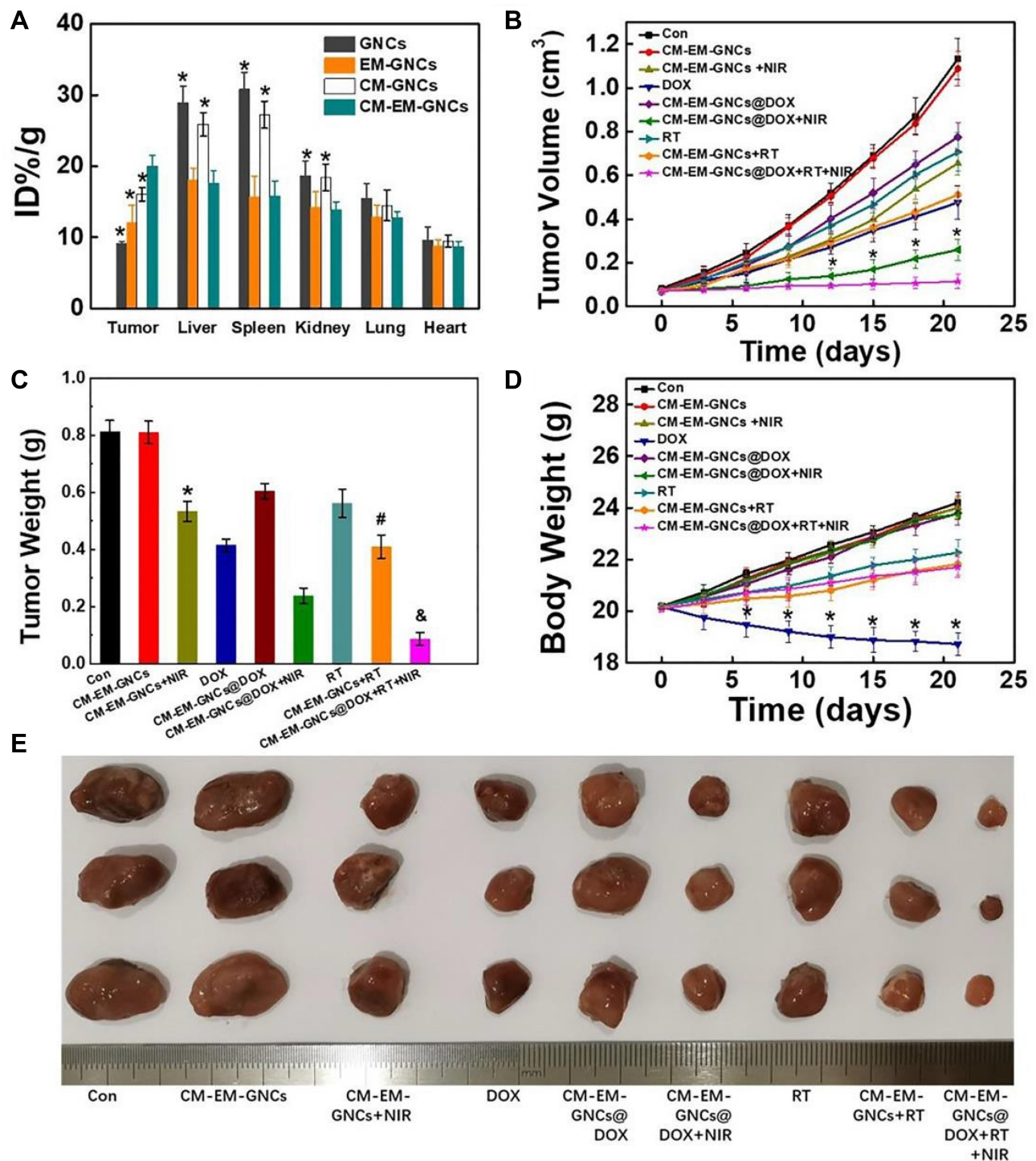


Figure 7 In vivo combined photothermal/radio/chemotherapy. (A) Quantitative ICP-OES analysis of GNCs, CM-GNCs, EM-GNCs and CM-EM-GNCs in the tumor, liver, spleen, kidney, lung and heart 24 h postinjection, * $P < 0.05$ vs the CM-EM-GNCs groups. (B) Tumor volumes, * $P < 0.05$ vs the CM-EM-GNCs@DOX+RT+NIR groups. (C) Tumor weights, * $P < 0.05$ vs the CM-EM-GNCs groups; # $p < 0.05$ versus RT groups; & $p < 0.05$ versus CM-EM-GNCs@DOX +NIR groups. (D) Body weights. * $P < 0.05$ vs the CM-EM-GNCs@DOX + RT+NIR groups. The data are presented as the mean values \pm SD; $n=3$. (E) Tumor photographs.

CM-EM-GNCs@DOX exhibited a 1.2-fold, 1.7-fold, and 2.2-fold higher accumulation in tumor tissues than CM-GNCs@DOX, EM-GNCs@DOX and GNCs@DOX, respectively, confirming the excellent homologous targeting ability to tumor tissues derived from the cancer membrane. The accumulation in the liver and spleen of CM-EM-GNCs@DOX was significantly decreased compared with that of CM-GNCs@DOX and GNCs@DOX. These results indicated that CM-EM-GNCs@DOX could be camouflaged by erythrocyte membranes to reduce the interception by liver and spleen. Then, we sought to evaluate the antitumor effect of CM-EM-GNCs@DOX in orthotropic MCF-7 nude mouse tumor models. As shown in Figure 7B, C and E, tumors in the CM-EM-GNC groups grew fast, which indicated that CM-EM-GNCs had few effects on tumor growth. When irradiated by NIR, CM-EM-GNCs exhibited an observable tumor growth inhibition, confirming the PTT efficacy of CM-EM-GNCs. In addition, CM-EM-GNCs@DOX showed a lower anti-tumor effect than free DOX due to the weak release of DOX without the assistance of NIR. When combined with

NIR, CM-EM-GNCs@DOX exhibited an outstanding inhibitory effect on tumor growth, indicating the excellent potential of CM-EM-GNCs@DOX on NIR-induced photothermal/chemotherapy. Moreover, single RT showed an unsatisfactory anti-tumor efficacy, whereas the radiotherapeutic effect was obviously improved after treatment with CM-EM-GNCs, further confirming the radiosensitization effect of our CM-EM-GNCs. As expected, CM-EM-GNCs@DOX plus NIR with RT exhibited the strongest anti-tumor effect. We next investigated the biosafety of these treatments. As shown in Figure 7D, the body weight was decreased in the RT groups and free DOX groups. Moreover, cardiotoxicity, which is known as a side effect of DOX, induced an increase in CK levels in the free DOX groups (Figure 8). Encouragingly, no observable pathological or serum biochemical index changes could be found in the CM-EM-GNCs@DOX plus NIR with RT treated groups (Figures 8 and 9). The weight loss of mice in the CM-EM-GNCs@DOX plus NIR with RT treated groups was obviously less than that in the free DOX groups. These results indicated

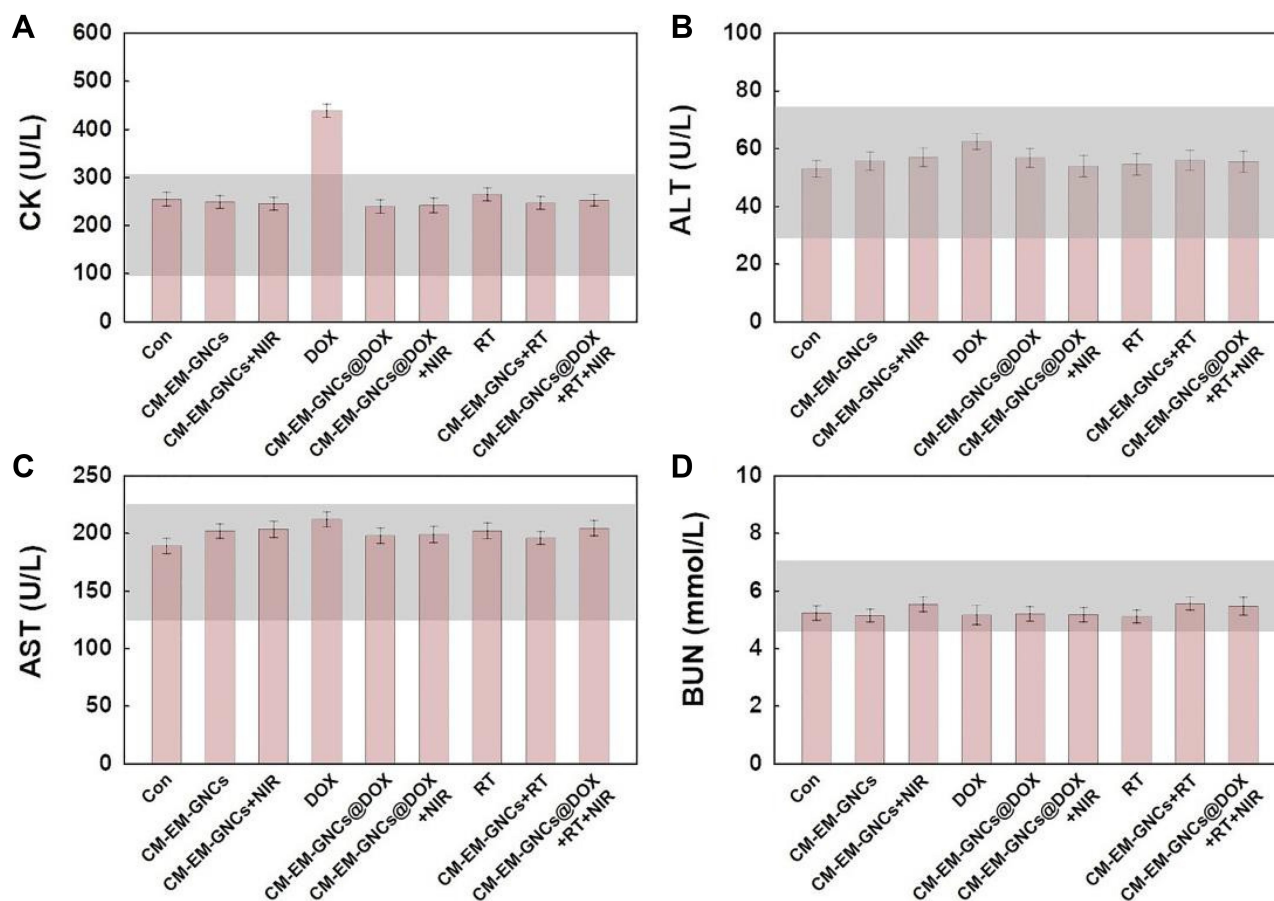


Figure 8 Serum biochemistry indicators included CK (A), ALT (B), AST (C) and BUN (D). The gray bars indicate the value range of healthy nude mice. The data are presented as the mean values \pm SD; n=3.

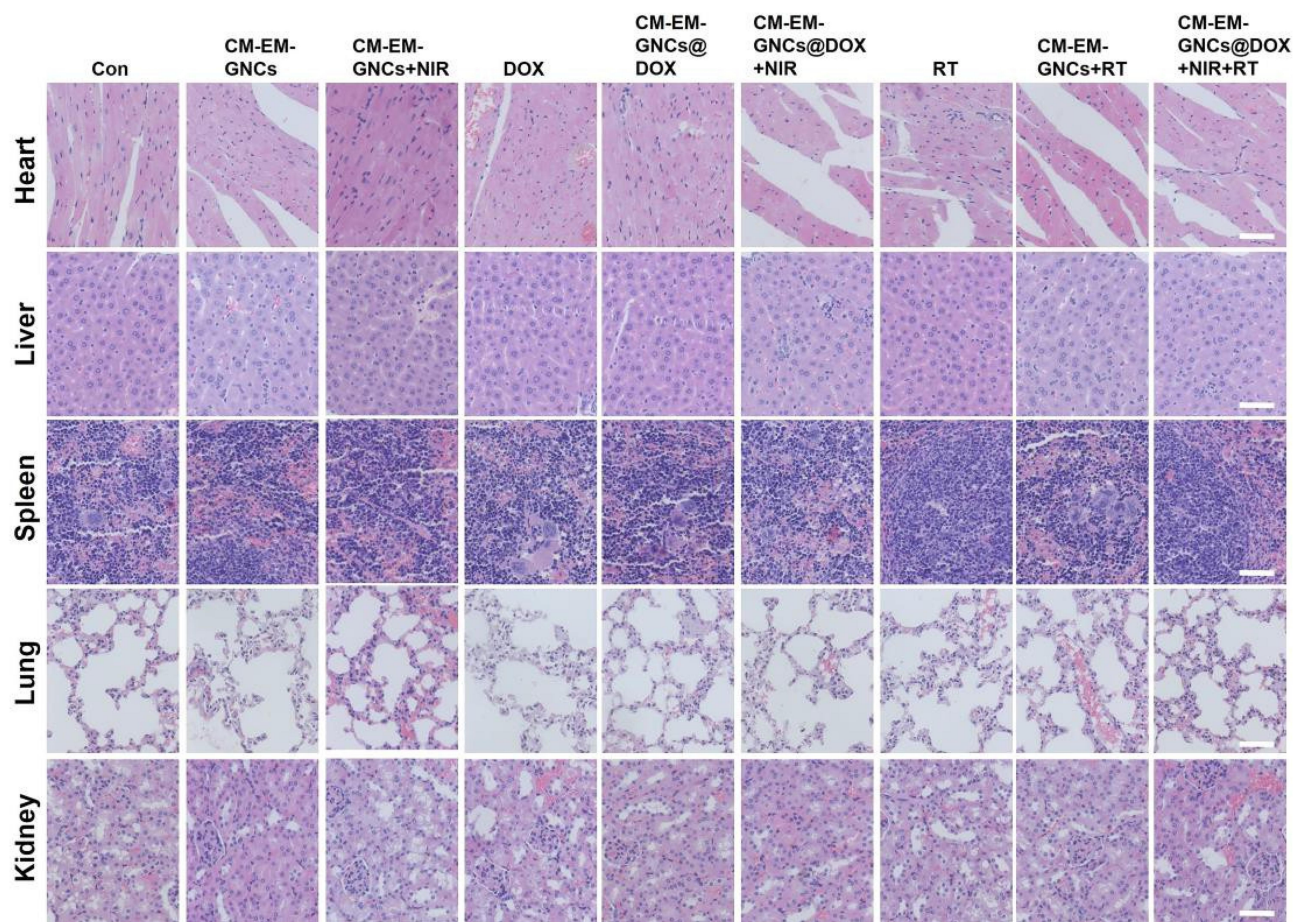


Figure 9 H&E staining images of the major organs from mice after various treatments. The scale bars represent 100 μm .

that CM-EM-GNCs@DOX could perform highly efficient combined photothermal/radio/chemotherapy with low side-effects.

Conclusion

In summary, we successfully fabricated cancer cell-erythrocyte hybrid membrane-coated doxorubicin (DOX)-loaded gold nanocages (CM-EM-GNCs@DOX) for combined photothermal/radio/chemotherapy of breast cancer. The CM-EM-GNCs@DOX exhibited a good photothermal conversion effect and NIR-responsive drug release behavior. Compared with bare GNCs, CM-EM-GNCs@DOX displayed high homologous targeting to MCF-7 cells and excellent immune evasion capabilities owing to the preserved characteristics derived from cancer cell membranes and erythrocyte membranes. High tumor accumulation and reduced interception in the liver and spleen were also demonstrated in orthotopic MCF-7 nude mice. Furthermore, CM-EM-GNCs@DOX displayed combined photothermal/radio/chemotherapeutic efficacy in vitro and in vivo experiments with few side effects. Therefore, our

prepared CM-EM-GNCs@DOX possessed a promising potential for highly efficient and safe treatment of breast cancer.

Acknowledgments

This work was supported by grants from the National Natural Science Foundation of China (81730074).

Disclosure

The authors report no conflicts of interest in this work.

References

1. Cristofanilli M, Budd GT, Ellis MJ, et al. Circulating tumor cells, disease progression, and survival in metastatic breast cancer. *N Engl J Med*. 2004;351(8):781–791. doi:10.1056/NEJMoa040766
2. Wagle N, Painter C, Anastasio E, et al. Abstract 5371: the metastatic breast cancer project: partnering with patients to accelerate progress in cancer research. *Cancer Res*. 2018;78:5371.
3. Sherry AD, Mayer IA, Ayalapeacock DN, Abramson VG, Rexer B, Chakravarthy AB. Combining adjuvant radiotherapy with capecitabine in chemotherapy-resistant breast cancer: feasibility, safety, and toxicity. *Clin Breast Cancer*. 2020;20(4):344–352.e1. doi:10.1016/j.clbc.2020.02.010

4. Wu X, Wu M, Jiang M, et al. TNF- α sensitizes chemotherapy and radiotherapy against breast cancer cells. *Cancer Cell Int.* 2017;17(1):13. doi:10.1186/s12935-017-0382-1
5. Klein JH, Tran WT, Watkins E, et al. Locally advanced breast cancer treated with neoadjuvant chemotherapy and adjuvant radiotherapy: a retrospective cohort analysis. *BMC Cancer.* 2019;19(1):306. doi:10.1186/s12885-019-5499-2
6. Krug D, Baumann R, Budach W, et al. Individualization of post-mastectomy radiotherapy and regional nodal irradiation based on treatment response after neoadjuvant chemotherapy for breast cancer. *Strahlenther Onkol.* 2018;194(7):607–618. doi:10.1007/s00066-018-1270-x
7. Lee JE, Park WS, Choi DH, et al. Patient-reported symptoms of radiation dermatitis during breast cancer radiotherapy: a pilot study. *Quality Life Res.* 2017;26(7):1713–1719. doi:10.1007/s11136-017-1526-4
8. Gibbs L, Bowen R, Makris A, Beresford M, Beresford M. Preferences for chemotherapy side-effect profiles in breast cancer – the view of oncologists. *Clin Oncol.* 2016;28(5):e3–e4. doi:10.1016/j.clon.2016.01.022
9. Her S, Jaffray DA, Allen C. Gold nanoparticles for applications in cancer radiotherapy: mechanisms and recent advancements. *Adv Drug Deliv Rev.* 2017;109:84–101. doi:10.1016/j.addr.2015.12.012
10. Yi X, Chen L, Zhong X, et al. Core-shell Au@MnO₂ nanoparticles for enhanced radiotherapy via improving the tumor oxygenation. *Nano Res.* 2016;9(11):3267–3278. doi:10.1007/s12274-016-1205-8
11. Wang Z, Chang Z, Shao D, et al. Janus gold triangle-mesoporous silica nanoplatfoms for hypoxia-activated radio-chemo-photothermal therapy of liver cancer. *ACS Appl Mater Interfaces.* 2019;11(38):34755–34765. doi:10.1021/acsami.9b12879
12. Li X, Wang Z, Wang X, et al. Berberine-loaded Janus gold mesoporous silica nanocarriers for chemo/radio/photothermal therapy of liver cancer and radiation-induced injury inhibition. *Int J Nanomedicine.* 2019;14:3967–3982. doi:10.2147/IJN.S206044
13. Yang Y, Zhu W, Dong Z, et al. 1D coordination polymer nanofibers for low-temperature photothermal therapy. *Adv Mater.* 2017;29(40):1703588. doi:10.1002/adma.201703588
14. Yang Y, Liu J, Liang C, et al. Nanoscale metal-organic particles with rapid clearance for magnetic resonance imaging-guided photothermal therapy. *ACS Nano.* 2016;10(2):2774–2781. doi:10.1021/acsnano.5b07882
15. Wang Y, Liu X, Deng G, et al. Se@SiO₂-FA-CuS nanocomposites for targeted delivery of DOX and nano selenium in synergistic combination of chemo-photothermal therapy. *Nanoscale.* 2018;10(6):2866–2875. doi:10.1039/C7NR09237G
16. Song M, Liu N, He L, et al. Porous hollow palladium nanoplatfom for imaging-guided trimodal chemo-, photothermal-, and radiotherapy. *Nano Res.* 2018;11(5):2796–2808. doi:10.1007/s12274-017-1910-y
17. Hainfeld JF, Lin L, Slatkin DN, Dilmanian FA, Vadas TM, Smilowitz HM. Gold nanoparticle hyperthermia reduces radiotherapy dose. *Nanomedicine.* 2014;10(8):1609–1617. doi:10.1016/j.nano.2014.05.006
18. Cheng H, Huo D, Zhu C, et al. Combination cancer treatment through photothermally controlled release of selenous acid from gold nanocages. *Biomaterials.* 2018;178:517–526. doi:10.1016/j.biomaterials.2018.03.058
19. Piao J, Gao F, Li Y, et al. pH-sensitive zwitterionic coating of gold nanocages improves tumor targeting and photothermal treatment efficacy. *Nano Res.* 2018;11(6):3193–3204. doi:10.1007/s12274-017-1736-7
20. Zhang A, Guo W, Qi Y, Wang J, Ma X, Yu D. Synergistic effects of gold nanocages in hyperthermia and radiotherapy treatment. *Nanoscale Res Lett.* 2016;11(1):279. doi:10.1186/s11671-016-1501-y
21. Huang S, Duan S, Wang J, et al. Folic-acid-mediated functionalized gold nanocages for targeted delivery of anti-miR-181b in combination of gene therapy and photothermal therapy against hepatocellular carcinoma. *Adv Funct Mater.* 2016;26(15):2532–2544. doi:10.1002/adfm.201504912
22. Wan J, Geng S, Zhao H, et al. Precise synchronization of hyperthermia-chemotherapy: photothermally induced on-demand release from injectable hydrogels of gold nanocages. *Nanoscale.* 2018;10(42):20020–20032. doi:10.1039/C8NR06851H
23. Wang Z, Zhang F, Shao D, et al. Janus nanobullets combine photodynamic therapy and magnetic hyperthermia to potentiate synergetic anti-metastatic immunotherapy. *Adv Sci.* 2019;6(22):1901690. doi:10.1002/advs.201901690
24. Tang W, Zhen Z, Wang M, et al. Red blood cell-facilitated photodynamic therapy for cancer treatment. *Adv Funct Mater.* 2016;26(11):1757–1768. doi:10.1002/adfm.201504803
25. Fang RH, Jiang Y, Fang JC, Zhang L. Cell membrane-derived nanomaterials for biomedical applications. *Biomaterials.* 2017;128:69–83. doi:10.1016/j.biomaterials.2017.02.041
26. Sun H, Su J, Meng Q, et al. Cancer cell membrane-coated gold nanocages with hyperthermia-triggered drug release and homotypic target inhibit growth and metastasis of breast cancer. *Adv Funct Mater.* 2017;27(3):1604300. doi:10.1002/adfm.201604300
27. Rao L, Meng Q, Huang Q, et al. Platelet-leukocyte hybrid membrane-coated immunomagnetic beads for highly efficient and highly specific isolation of circulating tumor cells. *Adv Funct Mater.* 2018;28(34):1803531. doi:10.1002/adfm.201803531

International Journal of Nanomedicine

Publish your work in this journal

The International Journal of Nanomedicine is an international, peer-reviewed journal focusing on the application of nanotechnology in diagnostics, therapeutics, and drug delivery systems throughout the biomedical field. This journal is indexed on PubMed Central, MedLine, CAS, SciSearch®, Current Contents®/Clinical Medicine,

Journal Citation Reports/Science Edition, EMBase, Scopus and the Elsevier Bibliographic databases. The manuscript management system is completely online and includes a very quick and fair peer-review system, which is all easy to use. Visit <http://www.dovepress.com/testimonials.php> to read real quotes from published authors.

Submit your manuscript here: <https://www.dovepress.com/international-journal-of-nanomedicine-journal>

Dovepress